

# INTERFACE FERROMAGNETISM IN A $\text{SrMnO}_3/\text{LaMnO}_3$ SUPERLATTICE

S. Smadici,<sup>1</sup> B.B. Nelson-Cheeseman,<sup>2</sup> A. Bhattacharya,<sup>2,3</sup> and P. Abbamonte<sup>1</sup>

<sup>1</sup>*Frederick Seitz Materials Research Laboratory, University of Illinois, Urbana, Illinois 61801*

<sup>2</sup>*Materials Science Division, Argonne National Laboratory, Argonne, Illinois 60439*

<sup>3</sup>*Center for Nanoscale Materials, Argonne National Laboratory, Argonne, Illinois 60439*

Resonant soft x-ray absorption measurements at the O  $K$  edge on a  $\text{SrMnO}_3/\text{LaMnO}_3$  superlattice show a shoulder at the energy of doped holes, which corresponds to the main peak of resonant scattering from the modulation in the doped hole density. Scattering line shape at the Mn  $L_{3,2}$  edges has a strong variation below the ferromagnetic transition temperature. This variation has a period equal to half the superlattice superperiod and follows the development of the ferromagnetic moment, pointing to a ferromagnetic phase developing at the interfaces. It occurs at the resonant energies for  $\text{Mn}^{3+}$  and  $\text{Mn}^{4+}$  valences. A model for these observations is presented, which includes a double-exchange two-site orbital and the variation with temperature of the hopping frequency  $t_{ij}$  between the two sites.

## I. INTRODUCTION

Doped  $\text{La}_{1-x}\text{Sr}_x\text{MnO}_3$  (LSMO) has multiple FM, AFM and canted magnetic orders as a function of doping and temperature<sup>1-3</sup> from superexchange<sup>6</sup> and double-exchange<sup>4,5</sup> interactions, which favor an antiferromagnetic (AFM) insulating phase and a ferromagnetic (FM) metallic phase, respectively. The FM phase at low temperatures is near the  $x = 0.33$  doping, at which the closely related manganite  $\text{La}_{1-x}\text{Ca}_x\text{MnO}_3$  shows very large (“colossal”) magnetoresistance (CMR)<sup>7</sup>.

The wave vectors of AFM and orbital orders in bulk manganites can be accessed with soft x-ray scattering at the Mn  $L_{3,2}$  edges. For instance, studies were made for  $\text{Pr}_{1-x}\text{Ca}_x\text{MnO}_3$  (Ref. 8),  $\text{La}_{2-x}\text{Sr}_x\text{MnO}_4$  (Refs. 9–11) and  $\text{La}_{2-2x}\text{Sr}_{1+2x}\text{Mn}_2\text{O}_7$  (Ref. 12) manganites. More recent measurements showed that magnetic and orbital scattering amplitudes are similar<sup>13</sup>, studied the doping dependence<sup>14</sup>, confirmed the separation in energy of Ref. 13 between the magnetic and orbital scattering resonances,<sup>15</sup> and studied their evolution after photoexcitation<sup>16</sup>. The broader features of the measurements are obtained in calculations of line shapes at the Mn  $L_{3,2}$  edges with atomic multiplet models of magnetic<sup>17</sup> and orbital<sup>18</sup> scattering, and more recently, with a finite-difference method<sup>19</sup>. However, the investigation of the bulk FM phase near the  $x = 0.33$  doping is not possible with soft x-ray scattering at the Mn  $L$  edges, due to lack of contrast for this order.

The FM phase can be studied with soft x-ray scattering in  $(\text{SMO})_n/(\text{LMO})_{2n}$  superlattices (SL), in which the Sr and La atoms are ordered in  $\text{SrMnO}_3$  (SMO) and  $\text{LaMnO}_3$  (LMO) layers. External magnetic fields are not necessary. The SL growth sequence can be used to define the period and symmetry of a reflection along the  $c$ -axis. This was demonstrated for a  $n = 4$  SL, in which the scattering wave vector was decreased to a range accessible at the O  $K$  edge resonance and a higher symmetry of a reflection used to probe interface scattering.<sup>20</sup>

In this work, we have applied these ideas to SL reflections at the O  $K$  and Mn  $L_{3,2}$  edges and studied the

development of the FM moment in a shorter superperiod  $n = 2$  SL with soft x-ray absorption and scattering. Measurements at the O  $K$  edge showed modulated hole doping at oxygen sites. We have observed scattering at the Mn  $L$  edges from the SL interfaces at SL reflection  $L = 2$ , following the temperature dependence of the FM moment. The symmetry of the SL reflection allowed us to probe all Mn valences in the interface layers. In addition to  $\text{Mn}^{3+}$  valence resonances of bulk AFM order measurements<sup>8-16</sup>, a peak in the resonant line shape, which has not been observed before, is aligned with the fluorescence yield edge for the  $\text{Mn}^{4+}$  valence. We present a model of the x-ray scattering from the SL interfaces, which includes the temperature dependence of the double-exchange hopping frequency  $t_{ij}$  and the change in the configurations of the Mn ions in the FM state.

## II. EXPERIMENTS

### A. Structure

The  $n = 2$  SL was grown on the (001) surface of  $\text{SrTiO}_3$  (STO) at Argonne National Laboratory at 700 °C in a  $2 \times 10^{-6}$  Torr ozone pressure, followed by cooling to 100 °C and pump down. The structure was  $\{r \times [2(\text{SMO}) + 4(\text{LMO})] + \text{SMO}\}$  with  $r = 13$  [Fig. 1(a)]. SMO ( $a_{\text{SMO}} = 3.805$  Å, Ref. 21) and LMO ( $a_{\text{LMO}} = 3.99$  Å, Ref. 22) layers on the STO substrate ( $a_s = 3.905$  Å) are under +2.6 % tensile and -2.2 % compressive strain. The surface RMS roughness, measured with an atomic force microscope, was  $\sigma_s = 2.85$  Å. From hard and soft x-ray reflectivity measurements, the SL superperiod was  $c_{\text{SL}} = 22.5 \pm 0.5$  Å and the average  $c$ -axis parameter for 1 ML (a coverage of one formula unit of SMO or LMO over a  $a_s \times b_s$  area) was  $3.86 \pm 0.05$  Å.

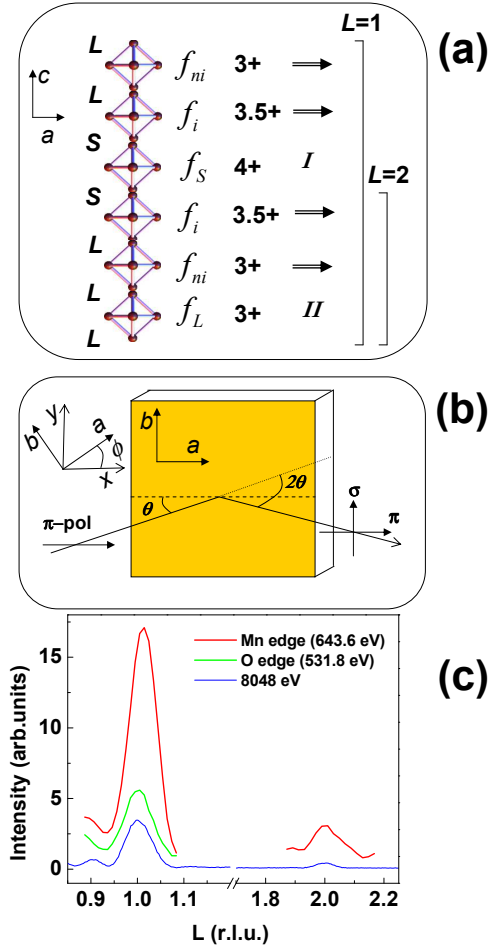


FIG. 1: (Color online) (a) Sketch of a 6 ML superperiod of the  $(\text{SMO})_2/(\text{LMO})_4$  superlattice with LaO ( $L$ ) and SrO ( $S$ ) planes, layer form factors  $f$ , Mn valences in the  $\text{MnO}_2$  planes estimated from the neighboring  $L$  or  $S$  planes, a magnetic order in the FM state and periods of the  $L = 1$  and  $L = 2$  SL reflections. (b) Scattering geometry for azimuth  $\phi = 0^\circ$ . The scattering vector is along the  $c$ -axis, normal to the surface. (c) SL momentum scans at the Mn  $L_3$ , O  $K$  edges and with hard x-rays (8048 eV).

## B. X-ray absorption

X-ray absorption spectroscopy (XAS) measurements in fluorescence (FY) and electron yield (EY) modes were made at undulator beamline X1B at the National Synchrotron Light Source. The incident light was  $\pi$ -polarized and the incidence and detector angles were  $\theta = 80^\circ$  and  $2\theta = 110^\circ$  [Fig. 1(b)]. The calculated energy resolution was 0.39 eV and 0.59 eV at O  $K$  (520 eV) and Mn  $L_3$  (640 eV) edges, respectively.

SL FY and EY measurements at the O  $K$  edge show doped holes on the oxygen sites (Fig. 2). Because the probing depth exceeds the total SL thickness, FY has contributions from both the SL and the substrate. In contrast, because of the short electron escape depth, EY measurements are from the SL top layers only. The should-

der in FY measurements at 530.3 eV is aligned with the first peak in EY and is not present in FY measurements of the bare STO substrate. This shoulder corresponds to doped holes in LSMO (Ref. 24) and to the  $L = 1$  scattering peak at 529.6 eV. The peak at 531.8 eV is from the STO substrate. The SL FY and EY measurements at the O  $K$  edge show no discernible variation with temperature between 300 K and 255 K.

SL FY and EY measurements at the Mn  $L_{3,2}$  edges are compared to FY measurements on bulk samples with different Mn valences (Refs. 25–27) in Fig. 3. SL FY does not have the sharp peak at the lower energies characteristic of the  $\text{Mn}^{2+}$  valence, which shows that the SL has only the  $\text{Mn}^{3+}$  and  $\text{Mn}^{4+}$  valences. The SL FY measurement was aligned in energy with the average of bulk FY for the  $\text{Mn}^{3+}$  and  $\text{Mn}^{4+}$  valences, according to the number of SMO ( $\text{Mn}^{4+}$  valence) and LMO ( $\text{Mn}^{3+}$  valence) layers in one superperiod. No discernible variation was observed in FY or EY between 300 K and 255 K.

XAS measurements probe the average valence of O and Mn atoms in the SL. To discern a variation with temperature in different SL layers it is necessary to turn to scattering.

## C. Resonant soft x-ray scattering

Resonant soft x-ray scattering (RSXS) measurements were made at the same beamline with an ultra-high vacuum diffractometer. For other RSXS experiments on bulk and SL at this endstation see Refs. 20,23,28–31. Detection was for both  $\pi - \pi$  and  $\pi - \sigma$  channels. The scattering momentum in the reflectivity geometry  $Q = (0, 0, 2\pi L/c_{SL})$  is indexed with respect to the SL superperiod  $c_{SL}$ . The energy resolution was 0.20 eV and 0.34 eV at O  $K$  (520 eV) and Mn  $L_3$  (640 eV) edges, respectively. The sample was cooled in zero magnetic field and scattering measurements for  $L = 1$  at the O  $K$  edge and for  $L = 1, 2$  at the Mn  $L_{3,2}$  edges [Fig. 1(c)] were made at different temperatures (Figs. 2 and 4).

FM order in metallic films has been studied with x-ray resonant magnetic scattering of linearly<sup>32</sup> and circularly<sup>33</sup> polarized light at the Fe and Co  $L$  edges. The FM order in a Ag/Ni SL has been investigated with circularly polarized light<sup>34</sup>. However, unlike previous studies, where an external magnetic field was applied to separate the magnetic and charge scattering, the SL FM order is accessed here at SL reflections with no applied magnetic fields.

### 1. O $K$ edge line shape

The spatial modulation in the density of holes doped on the oxygen sites can be observed with RSXS. Specifically, the O  $K$  edge line shape for  $L = 1$  scattering shows a peak close to the energy of the shoulder in FY measurements (Fig. 2).

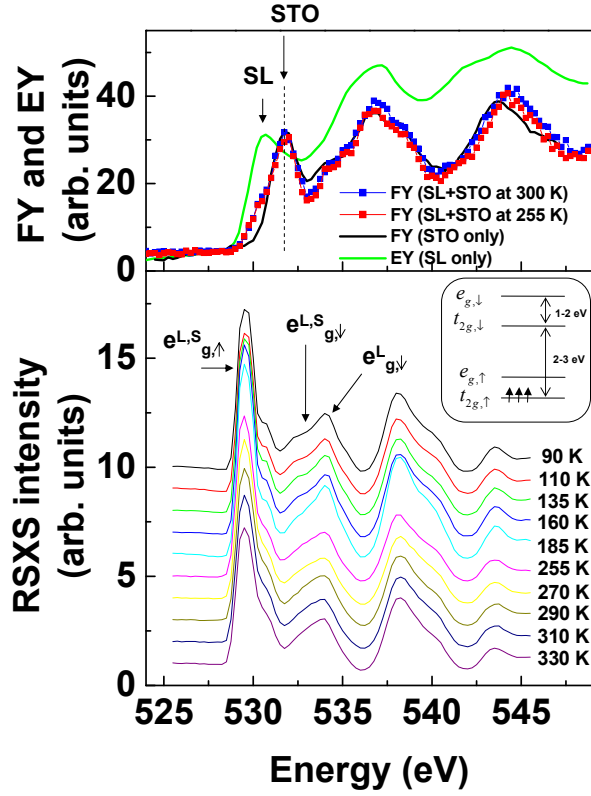


FIG. 2: (Color online) Top: FY at the O  $K$  edge for the SL on STO at different temperatures and the bare STO substrate (black line), compared to EY measurements. FY measurements were aligned with the linear transformation  $FY_{\text{plotted}} = aFY_{\text{measured}} + b$ , where  $a$  and  $b$  are constants. Bottom: Temperature dependence of resonant scattering at  $L = 1$ . The scans have been normalized to the pre-edge values and shifted vertically for clarity. The inset shows the order of the energy levels for SMO in the ground state, with the Jahn-Teller splitting neglected. The upper level  $e_{g,\downarrow}$  is split in LMO.

Since the order of levels in the RSXS line shape at the O  $K$  edge follows that of the ground state, the RSXS line shape can be analyzed using the hybridization between O  $p$  and Mn  $e_g$  levels in the ground state. XAS experiments and calculations at the Mn  $L$  edge (Ref. 35) give a crystal field splitting  $10Dq$  between the  $e_g$  and  $t_{2g}$  levels of 1.5 eV for bulk LMO and 2.4 eV for SMO. Fig. 2 (inset) shows the unoccupied  $e_{g,\uparrow}$ ,  $t_{2g,\downarrow}$  and  $e_{g,\downarrow}$  levels in SMO. The scattering line shape at the O edge is described well by O  $p$  states hybrids with the Mn  $e_g$  levels in the SMO and LMO layers, shown with arrows in Fig. 2, followed at higher energy by hybrids with La and Sr states. Two  $e_{g,\downarrow}$  levels (3.5 eV and 5 eV above  $e_{g,\uparrow}$ ) are present in LMO and only one for SMO (3.5 eV above  $e_{g,\uparrow}$ ) (Ref. 36) because the electron in the  $e_{g,\uparrow}$  level in LMO splits the unoccupied  $e_{g,\downarrow}$  levels by Coulomb interaction, even in the absence of any Jahn-Teller distortion.

However, no variation across the FM transition is observed within the error bars. To access T-dependent in-

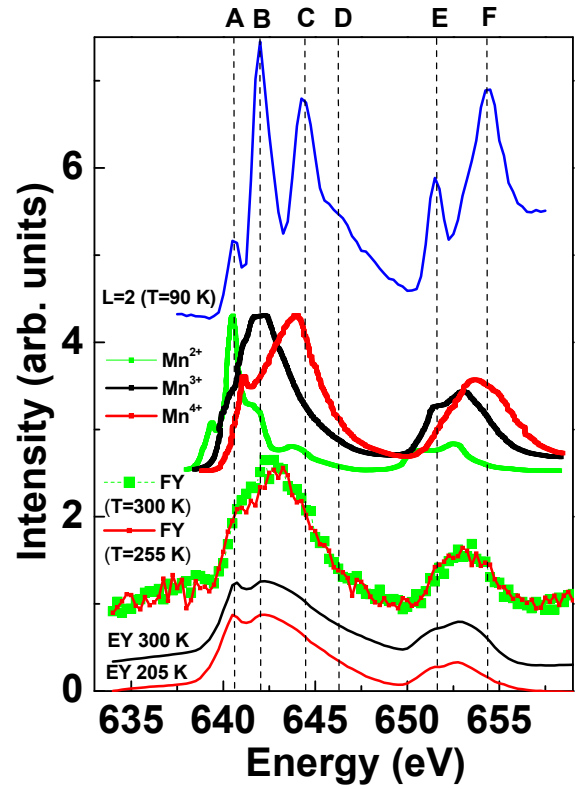


FIG. 3: (Color online) SL EY and FY (lower curves) and RSXS (top) at  $L = 2$  at the Mn  $L_{3,2}$  edges compared to FY measurements for different Mn valences (middle, from Ref. 26).

terface states (Sec. III A), it is necessary to reach the  $L = 2$  reflection, for which the O  $K$  edge energy is too low. In contrast,  $L = 2$  is accessible at the Mn  $L_{3,2}$  edges.

## 2. Mn $L_{3,2}$ edge valences

There is no discernible variation in the line shape at  $L = 1$  at the Mn  $L_{3,2}$  edges across the FM transition temperature (Fig. 4). However, a pronounced variation is visible for  $L = 2$ . From under the relatively broad XAS at the Mn  $L$  edge, T-dependent RSXS at  $L = 2$  selects those states that are sensitive to the temperature variation. Specifically, an increased intensity of the A, B and C peaks at lower T, and a decreased intensity of the  $\alpha$  peak is observed at the  $L_3$  edge (Fig. 4). Parallel variations occur at the  $L_2$  edge for peaks E, F and  $\beta$ . Similar results were obtained for azimuthal angle  $\phi = 45^\circ$  (Fig. 5), consistent with the azimuthal dependence of magnetic scattering. The temperature dependence of height and width of peak C are shown in Fig. 6.

Coulomb and exchange interactions for ground and RSXS excited states are different at the Mn  $L_{3,2}$  edges. An analysis of the RSXS line shapes based on ground state calculations, similar to that at the O  $K$  edge, cannot be made. However, both FY and RSXS measurements

probe excited states and FY measurements on bulk samples for different Mn valences will be used to identify the valence of scatterers for different resonances in the RSXS line shapes. This approach is supported by the relatively small difference in energy between RSXS resonances for scatterers of the same valence and different specific scattering contrasts ( $\lesssim 1$  eV between magnetic and orbital scattering for bulk measurements<sup>13,15</sup>) compared to the  $\sim 2$  eV separation in energy between the main FY features for different valences (Fig. 3).

FY measurements in Sec. II B showed that the  $\text{Mn}^{2+}$  valence is absent in the SL. The  $A$  and  $B$  resonances in the RSXS line shape for  $L = 2$  correspond to the  $\text{Mn}^{3+}$  valence, while resonance  $C$  lines up at the energy of FY edge for a  $\text{Mn}^{4+}$  valence. More T-dependent measurements on SL with different superperiods are needed before a quantitative discussion of peak  $\alpha$ .

### III. DISCUSSION

The model of Sec. III A relates the variation with temperature of the scattering contrast for  $L = 2$  and the absence of variation for  $L = 1$  to changes in the form factor  $\delta f_i$  of interface layers and interface ferromagnetism.

The variation of  $\delta f_i = f_{i,\text{FM}} - f_{i,\text{PM}}$  with the transition from the PM to the FM state for specific interface magnetic and orbital x-ray scattering models is discussed in Sec. III B.

#### A. Interface ferromagnetism

The line shape and structure factor at the Mn edge at  $L = 2$  (Fig. 4) are made of two parts. The T-independent structure factor  $S$  is given by the SL structure, to which a T-dependent contribution  $\delta S$  is added with the transition to the FM state [Fig. 6(a)].

The scattering intensity follows the evolution with temperature of the FM moment [Fig. 6(a)]. The possibility that the transition to the FM state gives exclusively non-magnetic scattering contrast is not supported by an analysis of the line shapes (Sec. III B). The T-dependent scattering  $\delta S$  is, at least partially, magnetic in origin and, for simplicity, we discuss only x-ray resonant magnetic scattering in this section. Orbital contributions to temperature variations in line shapes are addressed in Sec. III B.

The scattering intensity is  $I \propto |S + \delta S|^2$ . The scattering form factors  $(f)^{mn}$  and  $(\delta f)^{mn}$  are tensors, which are multiplied with the final ( $\hat{\epsilon}_f$ ) and initial ( $\hat{\epsilon}_i$ ) light polarization vectors. This gives an overall factor which, for charge ( $f$ ) and magnetic ( $\delta f$ ) scattering, is

$$S \propto \hat{\epsilon}_{f,m}^*(f)^{mn} \hat{\epsilon}_{i,n} \propto (\hat{\epsilon}_f^* \hat{\epsilon}_i) f(\omega) \quad (1)$$

$$\delta S \propto \hat{\epsilon}_{f,m}^*(\delta f)^{mn} \hat{\epsilon}_{i,n} \propto i[(\hat{\epsilon}_f^* \times \hat{\epsilon}_i) \hat{z}_l] \delta f(\omega) \quad (2)$$

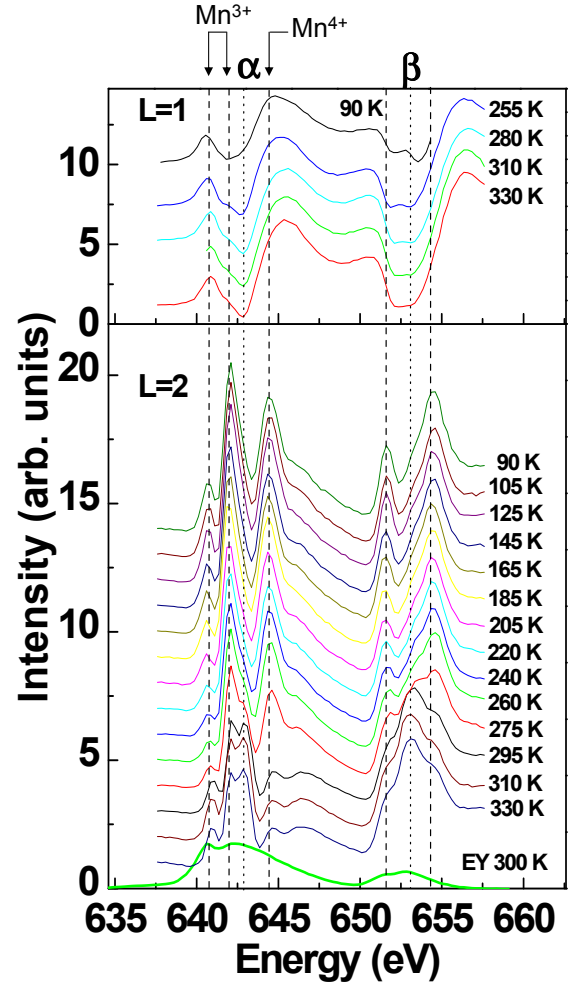


FIG. 4: (Color online) Temperature dependence of RSXS at the Mn  $L_{3,2}$  edges at  $L = 1$  and  $L = 2$  for azimuthal angle  $\phi = 0^\circ$ .

where  $\hat{z}_l$  is the direction of the local moment at site  $l$  (Refs. 32,34). The sum over the in-plane sites  $l$  for each layer is proportional to the magnetization  $\vec{M}$  of the layer.  $f(\omega)$  and  $\delta f(\omega)$  are scalar functions.

RSXS peaks that persist above the FM transition temperature are due to scattering contrast defined by the SL structure, which is held constant by the internal field between  $\text{Sr}^{2+}$  and  $\text{La}^{3+}$  ions arranged in the SL layers. With the form factors shown Fig. 1(a) for “interface” ( $f_i$ ), “near-interface” ( $f_{ni}$ ), “middle SMO” ( $f_S$ ) and “middle LMO” ( $f_L$ ) layers, and neglecting inter-diffusion roughness and structural differences between SMO/LMO and LMO/SMO interfaces, the T-independent structure factors  $S(Q) = \sum_l f_l e^{iQz_l}$  at  $L = 1, 2$  are

$$S(L = 1) = -f_L + f_S + f_i - f_{ni} \quad (3)$$

$$S(L = 2) = f_L + f_S - f_i - f_{ni} \quad (4)$$

The origin has been chosen so that an arbitrary phase factor between  $S(L = 1)$  and  $S(L = 2)$  is zero.

Higher momenta  $L$  are not accessible at the Mn  $L$



edges. However, the absence of a variation with temperature in the scattering intensity at  $L = 1$  [ $\delta S(L = 1) = 0$ ] and the variation at  $L = 2$  [ $\delta S(L = 2) \neq 0$ ] strongly suggests that the unit cell of the T-dependent contribution to the structure factor ( $\delta S$ ) is half the SL superperiod or 3 ML. The middle of the SMO and LMO layers (separated by 3 ML) are the most dissimilar parts of the SL structure, while the SMO/LMO and LMO/SMO interfaces (with two interfaces every superperiod, also separated by 3 ML) are similar. In the following, we consider a scattering component  $\delta S$  that develops at the SL interfaces.

These conditions are contrary to those expected for scattering from crystal field effects or structural differences in a SL, from either differences in the  $c$ -axis lattice constant or Jahn-Teller distortions, which do not have a 3 ML unit cell. In addition, no discernible variation was observed for scattering at the La  $M_{5,4}$  edges for  $L = 1$  or  $L = 2$  between 300 K and 225 K (data not shown). This shows that the change in the line shape is due to a variation with temperature in the resonant form factors of the SL layers ( $\delta f_l$ ), not of structural factors ( $\delta z_l$ ).

In addition, these symmetry conditions on  $\delta S$  set more stringent constraints on the variation of  $\delta f_l$  in the SL, beyond the experimental observation  $\delta S(L = 1) = -\delta f_L + \delta f_S + \delta f_i - \delta f_{ni} = 0$ . To obtain a 3 ML unit cell, the variation in the middle of the LMO and SMO layers must be equal,  $\delta f_L = \delta f_S$ . In addition, the variation in the interface and near-interface layers must be equal,  $\delta f_i = \delta f_{ni}$  [Fig. 1(a)].

FM order in the  $i$  and  $ni$  layers is consistent with estimates of the average Mn valence in a  $\text{MnO}_2$  plane based on the type ( $L$  or  $S$ ) of neighboring planes [Fig. 1(a)]. Specifically, a comparison to magnetic orders of equivalent bulk LSMO doping shows that  $\text{Mn}^{3+}$  and  $\text{Mn}^{3.5+}$  valences are near the FM dome for bulk LSMO. The magnitude of the FM moment depends on the Mn valence and implicitly on the SL interface roughness, with structural imperfections in a  $(\text{SMO})_{4.4}/(\text{LMO})_{11.8}$  SL correlating with the average interface FM moment.<sup>38</sup> However, the FM moment distribution is more symmetrical in the smaller superperiod  $n = 3$  SL (Ref. 39), consistent with the symmetric FM moment distribution in Fig. 1(a).

The 3 ML unit cell of T-dependent scattering shows that there must be two regions within a superperiod which are different from the FM  $i$  and  $ni$  layers. With one the middle of the SMO layers ( $f_S$ ), the other must be the middle of the LMO layers ( $f_L$ ). The x-ray scattering measurements imply that the magnetic scattering in these two layers is the same  $(\delta f_S)_{\text{mag}} = (\delta f_L)_{\text{mag}}$ . Therefore, these layers have either the same magnetization  $\vec{M}$  or no magnetization at low temperatures. The different hole doping of these layers does not support the possibility of an equal magnetization. The remaining possibility is that, as the SL is cooled and becomes FM in zero applied field, there is no magnetization in both these layers, or  $(\delta f_S)_{\text{mag}} = (\delta f_L)_{\text{mag}} = 0$ . Therefore, for the  $n = 2$  SL, the variation in magnetic scattering  $(\delta f)_{\text{mag}}$  and FM

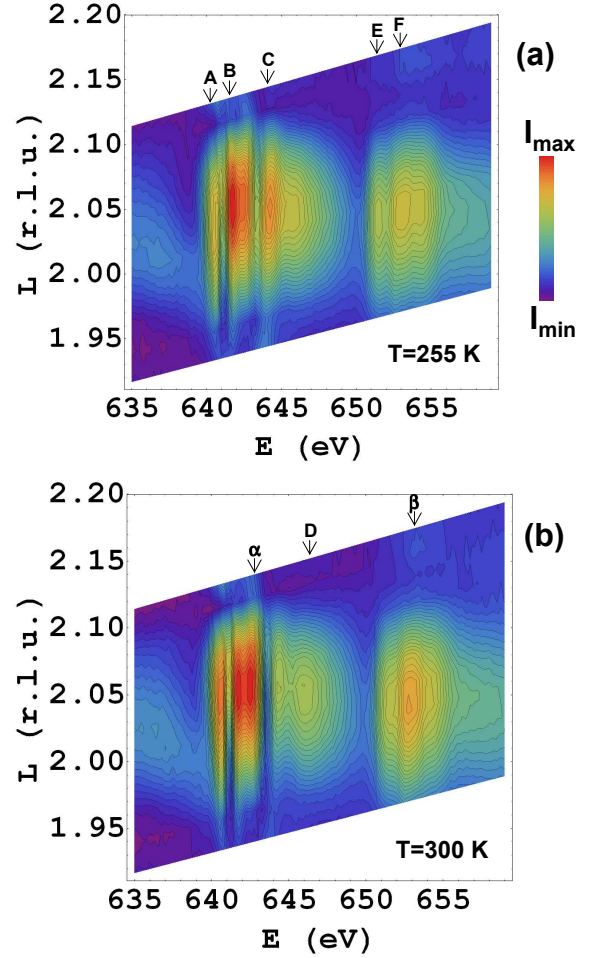


FIG. 5: (Color online) Two-dimensional resonance profiles at the Mn  $L_{3,2}$  edges at 255 K and 300 K for azimuth  $\phi = 45^\circ$ .

phase are localized at the SL interfaces.

A model of the magnetic state for the FM SL is shown in Fig. 1(a), where  $I$  and  $II$  represent magnetic phases of the  $f_S$  and  $f_L$  layers in no applied field (in contrast, the polarized neutron reflectivity measurements in Refs. 38,41 were made in applied fields). Since the average magnetization is zero for both  $I$  and  $II$  phases, the magnetic scattering has a 3 ML period. There are several different possible  $I$  and  $II$  phases: a PM phase, an ordered AFM phase (for instance, a C-type or a G-type), or an irregular phase with canted moments<sup>41</sup> pointing in different directions in the sample regions with slight variations in local doping<sup>3</sup>, even though the moments in the  $f_i$  and  $f_{ni}$  layers are always parallel.

The valences of the  $f_L$  and  $f_S$  layers are close to  $\text{Mn}^{3+}$  and  $\text{Mn}^{4+}$ , which correspond to A-type and G-type AFM magnetic orders in bulk LMO and SMO, with transition temperatures of  $T_{N,\text{LMO}} = 135$  K (Ref. 37) and  $T_{N,\text{SMO}} = 235$  K (Ref. 21), respectively. This suggests PM  $I$  or  $II$  phases, at least for the higher temperature range, below the SL FM transition temperature of 305 K [Fig. 6(a)]. However, the SL saturation

FM moment of  $\sim 2.5 \mu_B$  at 5 K (Ref. 40) gives the extent along the  $c$ -axis of the FM region in high fields of  $\gtrsim (2.5/3.22) \times 6 \text{ ML} \sim 4.65 \text{ ML}$  for each superperiod, where  $\sim 3.22 \mu_B$  is the maximum FM moment of the  $x = 0.33$  alloy<sup>39</sup>. This value is too high for both  $I$  and  $II$  phases to remain PM at the lowest temperatures. Therefore, at least one magnetic transition, other than the FM transition, occurs in the SL.

The RSXS measurements are consistent with transitions in the  $f_S$  and  $f_L$  layers from a PM phase at higher temperatures to either a G-type or C-type AFM phase (near the  $\text{Mn}^{4+}$  doping of bulk LSMO) and to an irregular canted phase (near the  $\text{Mn}^{3+}$  doping<sup>3</sup>) at lower temperatures, respectively. However, since there is no average layer magnetization in all these cases, the RSXS intensity does not vary at these transitions, in contrast to the FM transition in the  $i$  and  $ni$  layers.

With these constraints on  $\delta f_L$ , the change in the structure factor  $\delta S(Q) = \sum_l \delta f_l e^{iQz_l}$  at the FM transition and  $L = 1, 2$  from Eqs. (3)-(4) is

$$\delta S(L = 1) = 0 \quad (5)$$

$$\delta S(L = 2) = -2\delta f_i \quad (6)$$

Eq. (6) relates the changes with temperature in the line shape at  $L = 2$  to variations of form factor of interface  $\delta f_i$  and near-interface  $\delta f_{ni} = \delta f_i$  layers in the SL.

The  $\delta S(L = 2)$  reflection is allowed in this  $n = 2$  SL for all Mn sites in the FM layers. However, similar to AFM orders in bulk LSMO, scattering from a  $\text{Mn}^{4+}$  valence was not observed at  $L = 3$  for a  $n = 4$  SL (Ref. 20) [it was observed in a  $n = 3$  SL at  $L = 3$  (data not shown)]. The symmetry that very effectively forbids reflections from the  $\text{Mn}^{4+}$  ions at  $L = 3$  for the  $n = 4$  SL is not known and surprising, given inherent small imperfections of a SL structure. More measurements are needed for different SL to answer this question.

### B. Interface x-ray scattering

We now discuss the temperature variation of the RSXS line shape at  $L = 2$  and Mn  $L_{3,2}$  edges.

The width of resonance  $C$ , corresponding to the  $\text{Mn}^{4+}$  valence and to interface and near-interface layers, has a sharp increase at the FM transition temperature [Fig. 6(b)]. The increase in the scattering intensity in the FM state is also taking place  $\sim 0.2 \text{ eV}$  below the charge order resonance that corresponds to the  $\text{Mn}^{4+}$  valence in the PM state (at 644.65 eV in Fig. 4).

In general, the line shape of resonant magnetic scattering is related to variations in the occupation of orbitals induced by a magnetic field<sup>42</sup> near the FY edges for Mn ions of different ( $\text{Mn}^{3+}$  and  $\text{Mn}^{4+}$ ) valences. However, the magnetic scattering is slightly shifted to lower energies compared to orbital scattering for AFM bulk orders.<sup>13,15</sup> We cannot resolve two peaks at  $C$  in the SL line shapes at low T, but this suggests that, with the

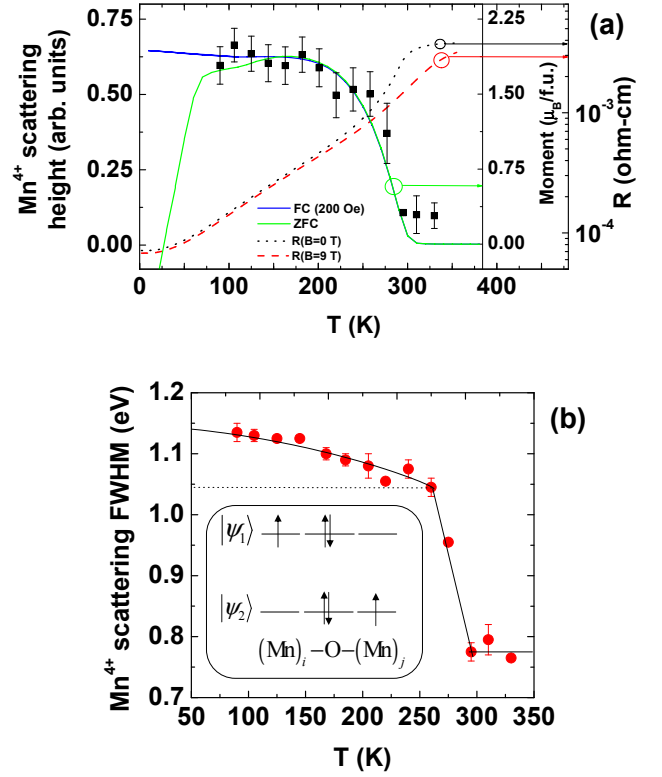


FIG. 6: (Color online) (a) Temperature dependence of resonance  $C$  height for  $\phi = 0^\circ$  compared to the SL FM moment measured with SQUID for ZFC and in-plane FC=200 Oe (Ref. 40). The SL has a  $305 \pm 5 \text{ K}$  FM transition temperature, which is lower than the  $\sim 355 \text{ K}$  transition temperature of the  $x = 0.33$  LSMO alloy (Ref. 39). Hysteresis loops show that the easy axis is in-plane (data not shown). SL resistance becomes metallic-like at low T (Ref. 40). (b) Temperature dependence of resonance  $C$  width. The line is a guide to the eye. Inset shows a sketch of the double-exchange configurations  $|\psi_1\rangle$  and  $|\psi_2\rangle$  for Mn sites  $i$  and  $j$  (Ref. 4).

increase of the FM moment at lower T, a T-dependent magnetic scattering contribution is added  $\sim 0.2 \text{ eV}$  below the charge scattering resonance. This addition to  $f_i$  of a temperature dependent  $(\delta f_i)_{\text{mag}}$  explains the observed variation in line shape at  $L = 2$ . The charge scattering resonance might also increase at lower T, concomitantly with magnetic scattering and variations in orbital scattering with T are discussed briefly at the end of this Section.

A more gradual increase in width is observed at lower T [Fig. 6(b)]. For x-ray scattering in the FM phase, it is necessary to consider a double-exchange two-site orbital, which suggests that this width increase is related to the T dependence of the double-exchange frequency  $t_{ij}$  between the two Mn sites. Both resonant magnetic and orbital scattering are ultimately scattering off orbitals, and the consideration of two-site orbitals in the FM state applies to both cases.

The double-exchange process involves two coordinated jumps from the Mn to the O atoms [Fig. 6(b), inset].

It is useful to consider the simpler process of one jump first, which is sometimes included in XAS calculations of complex oxides. In this case, inter-site charge transfer between  $d$ -states of a transition metal and a neighboring (ligand,  $L$ ) O ion<sup>43</sup> and consideration of multiple configurations (for instance,  $d^8$  and  $d^9\bar{L}$  for  $\text{Cu}^{1+}$  and  $\text{Cu}^{2+}$  valences) change the scattering form factor  $f$  at the transition metal edge. In particular, satellite peaks develop in XAS (and, implicitly, in RSXS) at additional Cu valences.<sup>44</sup>

In the double-exchange process, specific to FM complex oxides, charge transfer takes place between transition metal sites, beyond the neighboring O atoms. Specifically, the  $|\psi_1\rangle$  and  $|\psi_2\rangle$  configurations are coupled in a two-site ground state wave function [Fig. 6(b), inset], which for this FM manganite is

$$\begin{aligned} |\psi_{\pm}\rangle &= \frac{1}{\sqrt{2}}(|\psi_1\rangle \pm |\psi_2\rangle) \\ |\psi_1\rangle &= |\text{Mn}^{3+}, \text{O}^{2-}, \text{Mn}^{4+}\rangle \\ |\psi_2\rangle &= |\text{Mn}^{4+}, \text{O}^{2-}, \text{Mn}^{3+}\rangle \end{aligned} \quad (7)$$

with Mn valences in FM layers in a superposition of  $\text{Mn}^{3+}$  and  $\text{Mn}^{4+}$ . In the ground state (without an x-ray photon absorbed), the charge transfer splits the two levels  $|\psi_{\pm}\rangle$  by the exchange energy  $2t_{ij}$  (Ref. 4), where the double-exchange hopping between sites  $i$  and  $j$  is  $t_{ij} = t_{\text{DE}} \cos[(\theta_i - \theta_j)/2]$ , with  $t_{\text{DE}}$  a constant and  $\theta_{i,j}$  the  $t_{2g,\uparrow}$  spins orientations on the two sites (Ref. 5).

To account for the double-exchange process in x-ray scattering, the orbitals  $|\psi_{1,2}\rangle$  are replaced with the two-site orbitals  $|\psi_{\pm}\rangle$ . Similar to the case of ligand holes on oxygen atoms, the charge transfer between Mn sites beyond the neighboring O atoms changes the scattering factor  $f$  at satellite peaks in RSXS, which correspond to the  $\text{Mn}^{3+}$  and  $\text{Mn}^{4+}$  valences.

In addition, the splitting by  $2t_{ij}$  of the  $|\psi_{\pm}\rangle$  states results, for our relatively large energy resolution and core hole width, in an increase of the measured width by  $2t_{ij}$ . More precisely, the bandwidth of  $e_g$  electrons depends on the hopping frequency between the  $i$  and  $j$  sites as<sup>37</sup>

$$W \propto \cos[(\theta_i - \theta_j)/2] \cos\phi \propto t_{ij} \cos\phi \quad (8)$$

where  $(\pi - \phi)$  is the angle between the Mn-O-Mn bonds. A width increase at lower T in the ground state is transferred to a increase of the RSXS line width.

The hopping frequency  $t_{ij}$  increases with increased FM order of spins  $\theta_{i,j}$  at lower T, and broadens the scattering form factors  $f$  and the line width. In this model, the XAS and therefore, the RSXS peaks, should become broader at lower temperatures. The width increase at lower temperatures of peak  $C$  [Fig. 6(b)] is consistent with this model and  $t_{\text{band}} \sim 0.2 - 0.5$  eV for each of the  $e_g$  states,  $2t_{\text{DE}} \sim 2T_{\text{Curie}} \sim 0.05$  eV and contributions from experimental resolution (0.34 eV at the Mn  $L$  edge) and core-hole width ( $w_{\text{FWHM}} \sim 0.3 - 0.5$  eV, Ref. 8).

In addition to the double-exchange processes in the FM state, lattice distortions are also relevant to the CMR

transition<sup>45,46</sup>. In bulk manganites, they may depend on T, changing the bond alignment  $\phi$  and bandwidth  $W$  [Eq. (8)]. However, the average angle between the Mn-O-Mn bonds for SL samples is fixed by the substrate.

Orbital scattering at the Mn  $L$  edges has a comparable amplitude to magnetic scattering for bulk AFM orders.<sup>13,15</sup> It can come from occupation contrast or polarization contrast from different atomic orbital orientations in the anomalous scattering tensor. The analogous occupation contrast in SL FM is a T-dependent charge transfer across SL interfaces (which includes the electronic reconstruction of Ref. 20), in addition to the T-independent part defined by the SL structure. The T-dependent polarization contrast in the SL may also be substantial; for instance, on closely related SL (Ref. 47), in-plane  $e_g(x^2 - y^2)$  occupation and FM near LMO interfaces and out-of-plane  $e_g(3z^2 - r^2)$  orbital occupation and AFM in the middle of LMO layers was inferred from XMLD and XMCD measurements. Polarization-resolved scattering measurements in a magnetic field with  $\pi$  and  $\sigma$  incident light and scattered beam polarization analysis are necessary to separate different magnetic and orbital contributions to scattering at the Mn  $L_{3,2}$  edges.

We discuss the O  $K$  edge briefly. Oxygen doping is consistent with our observations (Fig. 2), other measurements<sup>24</sup> and certain models<sup>14</sup>. The interface FM state of this  $n = 2$  SL is the metallic state observed in a  $n = 4$  SL (Ref. 20). The reflection at  $L = 1$  (Fig. 2) is not sensitive to T-dependent scattering because, as for the Mn  $L$  edges,  $\delta S(L = 1) = 0$ . The intensity of the  $L = 3$  reflection in Ref. 20 corresponds to the  $L = 2$  reflection for this SL. In particular, to determine whether T-dependent scattering occurs at the O  $K$  edge in this SL, it would be necessary to measure at  $L = 2$ , a momentum which is not accessible at the O  $K$  edge.

#### IV. CONCLUSION

X-ray absorption measurements at the O  $K$  edge in a  $\text{SrMnO}_3/\text{LaMnO}_3$  superlattice showed a shoulder, corresponding to holes doped on oxygen sites. The shoulder is aligned with the main resonant peak of soft x-ray scattering from the spatial modulation in the density of doped holes.

A large variation in the Mn  $L_{3,2}$  line shapes at  $L = 2$ , but not at  $L = 1$ , was observed across the FM transition, pointing to scattering from ferromagnetic interfaces.

Comparison to fluorescence yield edge energies for different Mn valences showed the presence of scattering contrast at both  $\text{Mn}^{3+}$  and  $\text{Mn}^{4+}$  valences. An x-ray scattering model, which includes double-exchange orbitals in the FM state, explains the observed line broadening at lower temperatures.

Measurements on bulk 113 (Ref. 8), 214 (Ref. 9–11) and 327 (Ref. 12) manganites in the AFM state observe two main resonances only at the Mn  $L_3$  edge, at  $A$  and  $B$ . Scattering from  $\text{Mn}^{4+}$  ions (corresponding to res-

onance  $C$ ) has the symmetry of a forbidden reflection. Specifically, it has a spatial periodicity of 2 u.c. and is not allowed at the bulk in-plane orbital order reflection wave vector of 4 u.c. along the tetragonal axes (Ref. 8,9). Having to rely on measurements of the  $\text{Mn}^{3+}$  resonances only, different methods to determine the charge disproportionation for bulk AFM orders are controversial, with both small and large charge disproportionation obtained. Our RSXS line shapes, for a SL structure with a large intrinsic charge disproportionation, add an experimental constraint on these competing models.

The development of the SL FM order was accessed with x-ray resonant magnetic scattering and no applied magnetic fields. An open question is the trace [FC or ZFC in Fig. 6(a)] that the height of resonance  $C$  would follow on further cooling.

We would like to contrast our measurements to polarized neutron reflectivity (PNR) data on SMO/LMO superlattices (Refs. 38,41), where a magnetic modulation was measured with a period equal to the SL superperiod (magnetization strongly suppressed in SMO, high in LMO). In contrast, the RSXS measurements presented here show an ordering of magnetic moments with a period equal to half the SL superperiod. Several factors may be at the origin of this difference. First, the experimental

conditions of the PNR and RSXS measurements were different. Specifically, PNR measurements were made in relatively high fields (0.55 T and 0.82 T in Ref. 38 and 41, respectively), while the RSXS measurements were made with no applied fields. Second, the samples measured in this work have a lower SL superperiod ( $n = 2$ ) compared to the samples of PNR measurements ( $n = 3$  and  $n = 5$ ). Thus, a complete mapping of the magnetic structure of SMO/LMO superlattices as a function of deposition sequence, magnetic field and temperature requires more measurements.

## V. ACKNOWLEDGMENTS

This work was supported by the Department of Energy Office of Basic Energy Science: RSXS measurements by grant DE-FG02-06ER46285, NSLS facilities by DE-AC02-98CH10886, and MRL facilities by DE-FG02-07ER46453 and DE-FG02-07ER46471. Work at Argonne National Laboratory, including use of facilities at the Center for Nanoscale Materials, was supported by the U.S. Department of Energy, Office of Basic Energy Sciences under contract No. DE-AC02-06CH11357.

- 
- <sup>1</sup> E.O. Wollan and W.C. Koehler, Phys. Rev. **100**, 545 (1955).
  - <sup>2</sup> J.B. Goodenough, Phys. Rev. **100**, 564 (1955).
  - <sup>3</sup> P.-G. de Gennes, Phys. Rev. **118**, 141 (1960).
  - <sup>4</sup> C. Zener, Phys. Rev. **82**, 403 (1951).
  - <sup>5</sup> P.W. Anderson and H. Hasegawa, Phys. Rev. **100**, 675 (1955).
  - <sup>6</sup> P.W. Anderson, Phys. Rev. **79**, 350 (1950).
  - <sup>7</sup> S. Jin, T.H. Tiefel, M. McCormack, R.A. Fastnacht, R. Ramesh, and L.H. Chen, Science **264**, 413 (1994).
  - <sup>8</sup> K.J. Thomas *et al.*, Phys. Rev. Lett. **92**, 237204 (2004).
  - <sup>9</sup> S.B. Wilkins *et al.*, Phys. Rev. Lett. **91**, 167205 (2003).
  - <sup>10</sup> S.S. Dhesi *et al.*, Phys. Rev. Lett. **92**, 056403 (2004).
  - <sup>11</sup> S.B. Wilkins *et al.*, Phys. Rev. B **71**, 245102 (2005).
  - <sup>12</sup> S.B. Wilkins *et al.*, J. Phys.: Condens. Matter **18**, L323 (2006).
  - <sup>13</sup> U. Staub *et al.*, Phys. Rev. B **79**, 224419 (2009).
  - <sup>14</sup> M. Garcia-Fernandez *et al.*, Phys. Rev. B **82**, 235108 (2010).
  - <sup>15</sup> S.Y. Zhou *et al.*, Phys. Rev. Lett. **106**, 186404 (2011).
  - <sup>16</sup> H. Ehrke *et al.*, Phys. Rev. Lett. **106**, 217401 (2011).
  - <sup>17</sup> N. Stojic, N. Binggeli, and M. Altarelli, Phys. Rev. B **72**, 104108 (2005).
  - <sup>18</sup> C.W.M. Castleton and M. Altarelli, Phys. Rev. B **62**, 1033 (2000).
  - <sup>19</sup> O. Bunau, PhD thesis, University of Grenoble (2010).
  - <sup>20</sup> S. Smadici *et al.*, Phys. Rev. Lett. **99**, 196404 (2007).
  - <sup>21</sup> O. Chmaissem *et al.*, Phys. Rev. B **64**, 134412 (2001).
  - <sup>22</sup> J. Rodriguez-Carvajal *et al.*, Phys. Rev. B **57**, R3189 (1998).
  - <sup>23</sup> S. Smadici, J.C.T. Lee, J. Morales, G. Logvenov, O. Pelleg, I. Bozovic, Y. Zhu and P. Abbamonte, Phys. Rev. B **84**, 155411 (2011).
  - <sup>24</sup> H.L. Ju, H.-C. Sohn, and K.M. Krishnan, Phys. Rev. Lett. **79**, 3230 (1997).
  - <sup>25</sup> S. P. Cramer *et al.*, J. Am. Chem. Soc. **113**, 7937 (1991).
  - <sup>26</sup> F. Morales *et al.*, J. Phys. Chem. B **108**, 16201 (2004).
  - <sup>27</sup> J. Lee *et al.*, Phys. Rev. B **80**, 205112 (2009).
  - <sup>28</sup> P. Abbamonte, A. Rusydi, S. Smadici, G.D. Gu, G.A. Sawatzky, and D.L. Feng, Nature Physics **1**, 155-158 (2005).
  - <sup>29</sup> J.-S. Lee, C.-C. Kao, C.S. Nelson, H. Jang, K.-T. Ko, S.B. Kim, Y.J. Choi, S.-W. Cheong, S. Smadici, P. Abbamonte, and J.-H. Park, Phys. Rev. Lett. **107**, 037206 (2011).
  - <sup>30</sup> S. Smadici, J.C.T. Lee, S. Wang, P. Abbamonte, G. Logvenov, A. Gozar, C. Deville Cavellin, and I. Bozovic, Phys. Rev. Lett. **102**, 107004 (2009).
  - <sup>31</sup> S. Smadici, J.C.T. Lee, A. Rusydi, G. Logvenov, I. Bozovic, and P. Abbamonte, Phys. Rev. B **85**, 094519 (2012).
  - <sup>32</sup> C.C. Kao *et al.*, Phys. Rev. Lett. **65**, 373 (1990).
  - <sup>33</sup> C.C. Kao *et al.*, Phys. Rev. B **50**, 9599 (1994).
  - <sup>34</sup> J.M. Tonnerre *et al.*, Phys. Rev. Lett. **75**, 740 (1995).
  - <sup>35</sup> M. Abbate *et al.*, Phys. Rev. B **46**, 4511 (1992).
  - <sup>36</sup> T. Saitoh *et al.*, Phys. Rev. B **51**, 13942 (1995).
  - <sup>37</sup> J. Topfer *et al.*, J. of Solid State Chemistry **130**, 117 (1997).
  - <sup>38</sup> S. May *et al.*, Phys. Rev. B **77**, 174409 (2008).
  - <sup>39</sup> A. Bhattacharya *et al.*, Phys. Rev. Lett. **100**, 257203 (2008).
  - <sup>40</sup> B.B. Nelson-Cheeseman *et al.* (unpublished).
  - <sup>41</sup> T. Santos *et al.*, Phys. Rev. Lett. **107**, 167202 (2011).
  - <sup>42</sup> J.P. Hannon, G.T. Trammell, M. Blume, and D. Gibbs, Phys. Rev. Lett. **61**, 1245 (1988).
  - <sup>43</sup> F. de Groot, Coordination Chemistry Reviews **249**, 31



- (2005).
- <sup>44</sup> Z. Hu *et al.*, Chemical Physics **232**, 63 (1998).
- <sup>45</sup> H.Y. Hwang, S.W. Cheong, P.G. Radaelli, M. Marezio, and B. Batlogg, Phys. Rev. Lett. **75**, 914 (1995).
- <sup>46</sup> A.J. Millis, R. Mueller, and B.I. Shraiman, Phys. Rev. B **54**, 5405 (1996).
- <sup>47</sup> C. Aruta *et al.*, Phys. Rev. B **80**, 140405(R) (2009).